Exp Fluids (2008) 45:95–109
DOI 10.1007/s00348-008-0466-8

RESEARCH ARTICLE

Optical contouring of an acrylic surface for non-intrusive diagnostics in pipe-flow investigations

Benjamin J. de Witt · Haydee Coronado-Diaz · Ronald J. Hugo

Received: 23 October 2006 / Revised: 5 January 2008 / Accepted: 17 January 2008 / Published online: 9 February 2008

Abstract In this work, an acrylic surface was optically contoured to correct for the optical distortion caused by a transparent pipe wall. This method can be applied to non-invasive viewing/imaging techniques for fluid flow experiments. Software tools were developed to aid in the design of an optically contoured acrylic test section for pipe-flow experiments. Numerical models were computed for a standard acrylic pipe, inner diameter 57.15 mm, with water enclosed. An optical contour prototype was machined on a 5-axis CNC machine, and polished with 1–15 μm diamond paste, alleviating any surface imperfections without significantly altering the contoured surface. Experiments were then performed to measure the emerging optical wavefront and was found to emerge planar when utilizing the optical contour. It was determined that the wavefront was corrected to within ten wavelengths of a Helium–Neon (He–Ne) laser beam.

1 Introduction

Investigations of industrial flow systems such as piping networks, heat exchangers, or reactor vessels often rely upon non-invasive flow sensing methods for measuring velocity fields. Non-invasive flow sensing methods are comprised of modern diagnostic tools such as particle image velocimetry (PIV), laser Doppler velocimetry (LDV), optical tomography, or imaging with high-speed digital-video camera equipment. Curved surfaces, such as transparent pipe walls, cause significant distortions that degrade imaging capabilities. Figure 1 illustrates the degree of refraction caused by an acrylic pipe wall, where ray-tracing techniques (Klein 1970) have been used to compute light ray paths traveling through air into a transparent acrylic pipe filled with water. If non-invasive imaging techniques are to be used, modifications need to be made to correct for the optical distortions caused by curved surfaces. When conducting pipe-flow experiments, minimizing and preventing optical distortion caused by the acrylic pipe wall will involve one or a combination of the following correction methods reviewed by Steenbergen (1996):

1. Inverse manipulation of Snell's Law to augment refraction effects

   Boadway and Karahan (1981) and Bicen (1982) derive equations to find the actual location of a LDV probe volume and its angular orientation for different situations. Lowe and Kutt (1992) and Lowe et al. (1993) outline a correction procedure for three-dimensional image reconstruction of particle trajectories in flows through cylindrical tubes. The disadvantages of this method are that the enlargement of the LDV probe volume is not accounted for, and the receiving optics will require major realignments for each change of measurement location. Furthermore, total internal reflection of light may impede measurements in certain regions.

2. Placement of pipe within a transparent box

   Considerable enhancements are made by placing a pipe within a transparent box, filled with a fluid of

B. J. de Witt (✉) · H. Coronado-Diaz · R. J. Hugo
Department of Mechanical and Manufacturing Engineering, The University of Calgary, 2500 University Dr., N.W., Calgary, AB T2N 1N4, Canada
e-mail: bjdewitt@ucalgary.ca; bdewitt@gmail.com

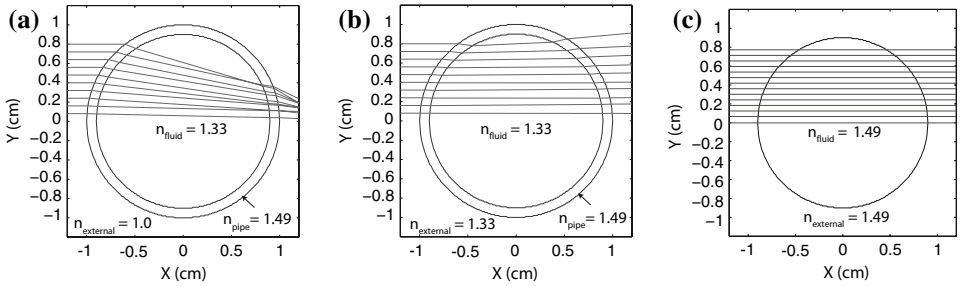

Fig. 1 Transparent pipe correction methods. **a** Optical distortions caused by acrylic pipe walls. **b** Fluid-in-box correction. **c** Index-matching correction

the same index of refraction as the fluid within the pipe. Studies performed by Chan et al. (2004),Westerweel et al. (1996), and Zhang (2004) use this correction method. Refraction effects are shown to be significantly improved, as shown by the computed beam paths in Fig. 1.

3. Refractive-index matching

   By matching the index of refraction of the fluid within a pipe to the index of refraction of the pipe-wall material, refraction effects are eliminated. This approach was used in investigations performed by Dybbs and Edwards (1987), Pereira and Sousa (1999), Uzol et al. (2002), and Agrawal et al. (1978). The latter investigation focused on the problem of flow development in curved pipes, where glycerin and water were mixed to closely match the refractive index of Plexiglas. Once more, a ray trace shown in Fig. 1 reveals the optical distortion for this situation. Some disadvantages of this solution include the need to control the temperature of the fluids in order to maintain the desired optical quality, the high viscosity of these fluids relative to water, and the need to machine a pipe section out of a cuboid portion of acrylic.

4. Thin versus thick pipe walls

   Reduction in pipe wall thickness leads to a smaller amount of refraction. Researchers at Physikalisch-Technische Bundesanstalt crafted a pipe test section with thin outer glass windows 100 μm thick. Laser Doppler velocimetry was then used to investigate pipe flows and installation effects (Wendt et al. 1996). This technique is modified in similar studies that have been performed substituting prefabricated flexible transparent films in place of manufactured pipe sections (Maanen and Fortuin 1983; Mizushina and Usui 1977; Steenbergen 1996). This method requires that flows be studied at low pressures due to the thin membrane, a limitation that obviously has drawbacks for certain applications.

5. Corrective lens

   A lens is introduced to compensate for the optical effects caused by a curved surface, such as a pipe wall. Applications of this method for LDV experiments are discussed in detail by Durrett et al. (1985) and Els and Rouve (1985).

An unconventional correction method involves custom machining an acrylic contour to remedy the optical distortions that occur in pipe-flow investigations. Laskowski et al. (2005) used this method for PIV experiments on a turbomachinery cascade where wall curvature effects were present, but not as severe as for pipe-flow experiments. This method of correction is referred to as "optical contouring," and it differs from the effect of a conventional lens. A lens is a device that causes light to either converge or to diverge (Giancola 1984). The optical contour designed in this work corrects for refraction caused by a clear pipe wall and the fluid within, and the goal is to produce an optical wavefront that emerges from the pipe wall planar. Optical contouring is an alternative correction method to the methods described earlier, with the potential for application in non-invasive flow sensing experiments involving collimated laser light such as optical wavefront sensing (McMackin et al. 1995) and optical tomography (McMackin et al. 1999). This paper also evaluates the performance of the optical contour while imaging objects within the pipe under ambient light conditions.

This paper will outline in several sections the design methodology, evaluation, and application of an optical contour to pipe-flow experiments. Section 2 introduces relevant background including Huygens' principle and quantifying wavefront distortions. Section 3 details the development of software tools that utilize ray-tracing techniques (Klein 1970) to determine the shape of an acrylic optical contour that corrects refraction due to the curvature of the acrylic pipe wall. Section 4 explains how the optical contour was manufactured. Section 5 discusses the verification of the optical contour design. Section 6 provides recommendations for future work and conclusions.

2 Theory and background

There are four models that may be considered when analyzing the propagation of an optical signal through an optical system: quantum optics; electromagnetic wave theory; scalar wave theory; and geometric optics (Welford 1991). Scalar wave theory considers the optical signal as an electromagnetic wave, whereas the geometric optics model regards light as bundles of rays that travel in straight lines. These two models may be linked through Huygens' principle, and both are useful in the present investigation.

2.1 Huygens' principle

A wavefront is defined as the locus of all points at which the phase of vibration of a physical quantity is the same. Huygens' principle states that *every point on a wavefront can be considered as a source of tiny wavelets that spread out in the forward direction at the speed of the wave itself; the new wavefront is the envelope of all the wavelets* (Giancola 1984). This is illustrated in Fig. 2, showing a wavefront traveling away from a source *S*. The wavefront at a later time is shown to be comprised of a series of secondary wavelets defining the new position of the wavefront. The notion of light rays follows from this concept, as being *directed perpendicular to the surface occupied by the wavefront at a given time* (Klein 1970). In other words, Huygens' principle maintains that light rays are always perpendicular to the optical wavefront.

Through a geometry exercise, the deflection angle of a light ray is equal to the local spatial derivative of the optical wavefront, as shown in Fig. 3. Hence, if a light ray is sent through an optical system, the deflection of the beam would provide knowledge of the slope of the wavefront at that spatial location where the light ray exits the aberrated media. This is useful for the current investigation

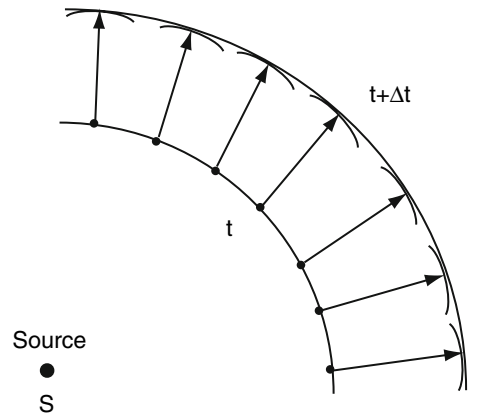

Fig. 2 Huygens' principle (Giancola 1984) used to determine shape of optical wavefront

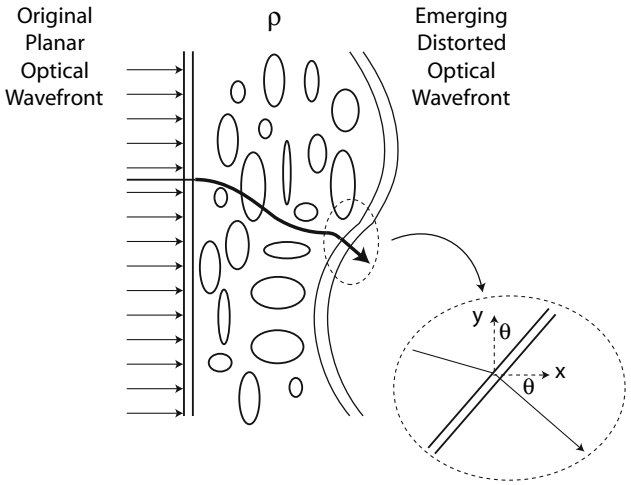

Fig. 3 Linking wavefront distortion with geometric and scalar optics models (ρ = density of the material)

because knowing the off-axis angle of a beam transmitted through an optical system, it is possible to quantify the distortion of the emerging optical wavefront (Jumper and Fitzgerald 2001).

2.2 Quantifying wavefront distortion

The spatial distortion of an optical wavefront may be described in two ways after it has transmitted through an optical system: optical path length (OPL) and optical path difference (OPD). For a known $n(x)$, the OPL can be calculated using:

$$\mathrm{OPL}(y) = \int_{x_1}^{x_2} n(x)\mathrm{d}x \tag{1}$$

where $n(x)$ is the index-of-refraction field along the path that the light travels. The index-of-refraction field can be found by knowing the thickness and index of the material that the light is propagating through. With this field known, the OPL can be evaluated at a number of points in the viewing aperture of the optical system. The OPD can be calculated by removing the spatial average of the OPL across the entire viewing aperture from the OPL itself. This is given as:

$$\mathrm{OPD}(y) = \mathrm{OPL}(y) - \mathrm{OPL}_{\mathrm{ave}} \tag{2}$$

where $\mathrm{OPL}_{\mathrm{ave}}$ denotes the spatial average of the OPL performed over the entire viewing aperture. Although OPD is used to quantify the spatial distortion of an optical wavefront, the OPD is not equal to the optical wavefront. Rather, the OPD is the *conjugate* of the optical wavefront. In order to minimize abberations the OPD must be zero across the viewing aperture. In effect, the emerging optical

wavefront is then planar. The shape of the optical contour may be solved for knowing that the OPD of the emerging wavefront must be zero.

3 Design methodology of optical contour

The outer wall shape required to correct for optical aberrations due to the curved surface of a pipe and an enclosed liquid may be computed from Snell's law of refraction and ensuring that the OPD is zero for the emerging wavefront. This section details two software tools that were developed to predict and verify the shape of the optical contour. They include: (1) the *optical contour calculator* (OCC) described in Sect. 3.1; and, (2) *ray-tracker* described in Sect. 3.2. The algorithms are developed in reference to a water-filled acrylic pipe.

3.1 Optical contour calculator

The first stage in this study concerns the development of software to calculate the shape of the optical contour. A functional breakdown of this algorithm is outlined in Fig. 4. The OCC algorithm may be broken into three sections:

1. Ray-trace through a pipe filled with water

   Compute the direction and OPL of light rays propagating through an acrylic pipe filled with water.

2. "Zeroing" angular deflection

   Compute the angle of a correction material such that the angle of the light rays are "zeroed" when emerging from the acrylic pipe and optical contour assembly.

3. "Zeroing" emerging wavefront

   Compute the thickness of the correction material such that the OPD of the emerging wavefront is zero. This ensures the emerging optical wavefront is planar.

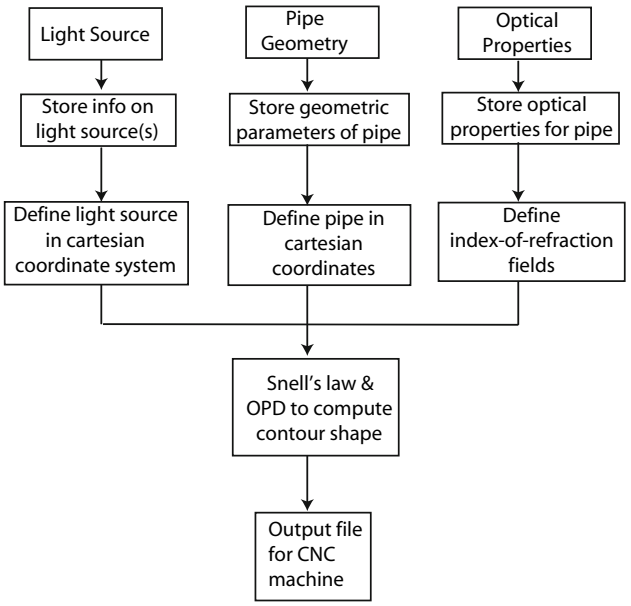

Fig. 4 Functional decomposition of optical contour calculator (*OCC*)

3.1.1 Ray-trace through a pipe filled with water

In the following derivation, a set of collimated beams are assumed to emerge from the center of the pipe. Due to the symmetry of the problem, computations will be performed in the first quadrant only. The symbol convention for these calculations is given in Fig. 5, where a section of a pipe in the first quadrant is shown. In the calculation, a beam is propagating parallel to the positive x-axis from a source that is located on the y-axis (x_0,y_0). Note that in the coordinate system defined in Fig. 5, the origin is defined at the center of the acrylic pipe.

The following two equations describe all points that lay on either the inner or outer pipe wall:

$$x_1^2 + y_1^2 = R_i^2 \tag{3}$$

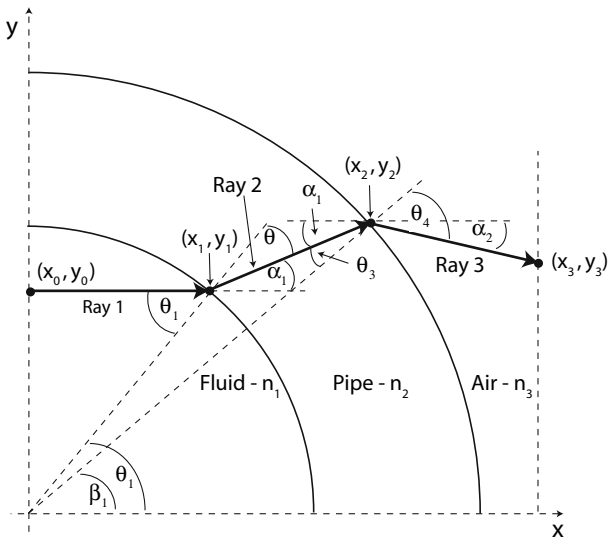

Fig. 5 Symbol conventions for ray-trace through a pipe filled with water

$$x_2^2 + y_2^2 = R_o^2 \tag{4}$$

where the subscripts i and o denote "inner" and "outer." The beam reaches the inner pipe wall at point (x_1, y_1), thus the angle θ_1 can be calculated:

$$\theta_1 = \tan^{-1}\left(\frac{y_1}{x_1}\right) \tag{5}$$

By Snell's Law, θ_2 can also be solved for:

$$\theta_2 = \sin^{-1}\left(\frac{n_1}{n_2}\sin\theta_1\right) \tag{6}$$

where n_1 is the refractive-index of water, and n_2 is the refractive-index of acrylic. The direction of a refracted light ray, shown as Ray 2 in Fig. 5 propagating through the acrylic section of pipe, is θ_2. The direction of this refracted light ray can also be described with respect to the x-axis, α_1, shown in Fig. 5:

$$\alpha_1 = \theta_1 - \theta_2 \tag{7}$$

The intersection of Ray 2 with the outer pipe wall can be computed by solving the following system of equations:

$$y_2 - y_1 = \tan(\alpha_1)\cdot(x_2 - x_1) \tag{8}$$

$$x_2^2 + y_2^2 = R_o^2 \tag{9}$$

where (x_1,y_1), α_1, R_o are known; (x_2,y_2) are unknown. Considering only the positive root when solving this system of equations, expressions for x_2 and y_2 are given as:

$$x_2 = \frac{-2y_1\tan(\alpha_1) + 2x_1\tan(\alpha_1)^2 + 2\zeta}{2\left(\tan(\alpha_1)^2 + 1\right)} \tag{10}$$

$$\zeta = \sqrt{R_o^2\tan(\alpha_1)^2 + 2x_1y_1\tan(\alpha_1) - y_1^2 - x_1^2\tan(\alpha_1)^2 + R_o^2} \tag{11}$$

$$y_2 = \sqrt{R_o^2 - x_2^2} \tag{12}$$

Thus, Ray 2 intersects the outer pipe wall at (x_2,y_2). The angle β_1 is solved for by taking the arctangent of the ratio of these coordinates:

$$\beta_1 = \tan^{-1}\left(\frac{y_2}{x_2}\right) \tag{13}$$

β_1 is used to compute the incident angle, θ_3, that Ray 2 makes with the normal at (x_2, y_2):

$$\theta_3 = \beta_1 - \alpha_1 \tag{14}$$

Once again, using Snell's law, θ_4 can then be solved for:

$$\theta_4 = \sin^{-1}\left(\frac{n_2}{n_3}\sin\theta_3\right) \tag{15}$$

The angle, α_2, describing the direction of Ray 3, is shown to be:

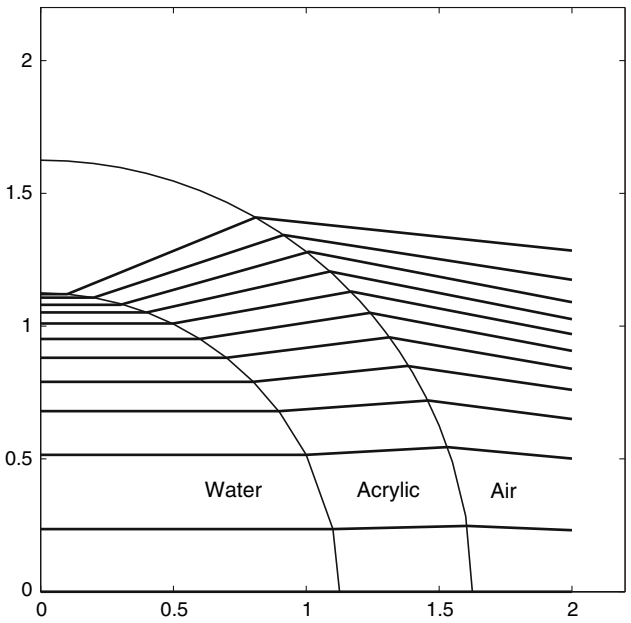

Fig. 6 Ray-trace for an acrylic pipe filled with water (R_i = 28.575 mm, R_o = 41.275 mm,12.7 mm wall thickness)

$$\alpha_2 = \beta_1 - \theta_4 \tag{16}$$

In order to complete the ray-trace, the ray must intersect with a plane that is perpendicular to the original ray direction and parallel to the pipe axis. This calculation can be performed for any plane in the x-direction, provided that it is greater than the outer radius of the pipe ($x_3 > R_o$). The point of intersection (x_3, y_3) can be computed by solving the following system of equations:

$$y_3 - y_2 = \tan(\alpha_2)(x_3 - x_2) \tag{17}$$

$$x_3 = x_f \tag{18}$$

where x_2, y_2, α_2, and x_f are known and y_3 is solved for. In this calculation, Ray 3 was chosen to intersect with the vertical plane at x_f = 50.8 mm. These calculations were repeated for several rays of light at different y-axis positions within the pipe. This method is known as a "ray-trace." Figure 6 illustrates a ray-trace for an acrylic pipe filled with water. Knowing the coordinates that describe Ray 1, Ray 2, and Ray 3, the OPL and the OPD can then be computed. This is an important boundary condition when calculating the thickness of the optical contour, and will be outlined in the next section.

3.1.2 *"Zeroing" angular deflection*

When light passes through the acrylic-air interface, illustrated in Fig. 7 as Ray 2, some correction material must turn the light ray such that it becomes parallel to the x-axis.

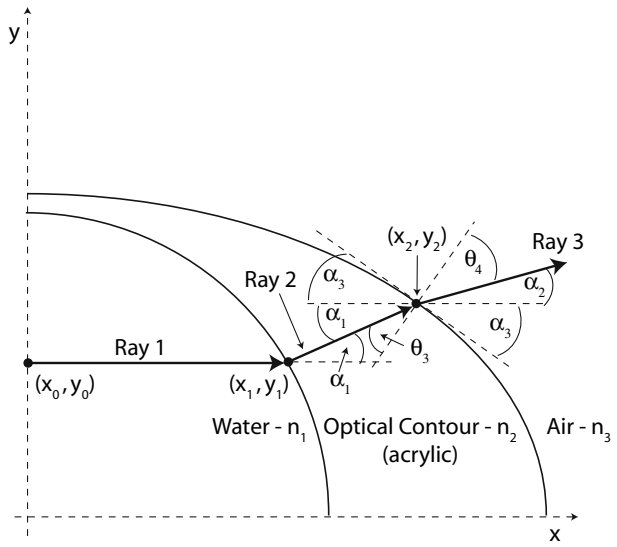

Fig. 7 Symbol convention used when "zeroing" vertical deflection

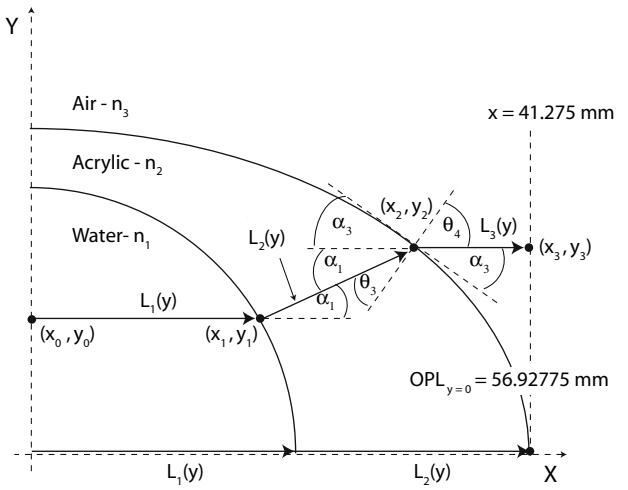

Fig. 8 Symbol convention used when "zeroing" emerging wavefronts

The following calculations "zero" a light ray with the x-axis, with no consideration being given to the thickness of the correction material. The thickness of the correction material will eventually be determined by the boundary condition OPD = 0 for the emerging wavefront. This calculation is performed in Sect. 3.1.3.

Rays of light, shown in Fig. 7 as Ray 2, will intersect with some additional material, referred to as the "optical contour." The refractive-index of this material is matched to acrylic $n = 1.49$. The following equations can be derived from the geometry shown in Fig. 7:

$$\theta_3 = \frac{\pi}{2} - \alpha_1 - \alpha_3 \tag{19}$$

$$\alpha_2 = \frac{\pi}{2} - \alpha_3 - \theta_4 \tag{20}$$

$$n_2 \sin(\theta_3) = n_3 \sin(\theta_4) \tag{21}$$

where α_2 must be zero for the light ray to emerge parallel to the x-axis. While elegant methods of finding a solution are available, a simple way of finding the solution is to guess a series of values of α_3. The correct value of α_3 is that which yields $\alpha_2 = 0$. The angle α_3 defines the slope of the optical contour at (x_2,y_2), determined independently from neighboring points. A program written in Microsoft Visual Basic was used to iterate a solution for a group of light rays. The next section will describe the method of calculating the thickness of the correction material.

3.1.3 *"Zeroing" emerging wavefront*

The emerging wavefront from the pipe was desired to be planar for experiments that involved applying optical wavefront sensing to pipe flow (Bertola 2004). In order for the wavefront to be planar, the OPD of the emerging wavefront must be zero. From Eq. 2, it is required that OPL(y) be equal across the entire viewing aperture for the OPD to be zero. This boundary condition will allow the thickness of the correction material to be determined. Figure 8 illustrates part of the symbol convention for this problem.

The OPL of a light ray traveling through the center of the pipe, $y = 0$, is:

$$\mathrm{OPL}_{y=0} = \int_{s_1}^{s_2} n(s)\mathrm{d}s = L_1(y_0)n_{\text{water}} + L_2(y_0)n_{\text{acrylic}} \tag{22}$$

This is the largest OPL of any beam traversing the pipe. Knowing the value for the OPL, the coordinates (x_2,y_2) of the optical contour may be solved for numerically. The following equations were derived using the geometry presented in Fig. 8:

$$\mathrm{OPL}(y) = L_1(y)n_1 + L_2(y)n_2 + L_3(y)n_3 \tag{23}$$

$$L_1(y) = \sqrt{(x_1 - x_0)^2 + (y_1 - y_0)^2} \tag{24}$$

$$L_2(y) = \sqrt{(x_2 - x_1)^2 + (y_2 - y_1)^2} \tag{25}$$

$$L_3(y) = \sqrt{(x_3 - x_2)^2 + (y_3 - y_2)^2} \tag{26}$$

$$y_3 - y_2 = \tan(\alpha_2)(x_3 - x_2) = 0 \tag{27}$$

$$x_3 = x_f \tag{28}$$

$$y_2 - y_1 = \tan(\alpha_1)(x_2 - x_1) \tag{29}$$

where OPL(y) = 56.93 mm. OPL(y) was calculated using Eq. 22, assuming a pipe wall thickness of 12.7 mm. The variable x_f was determined from the inner diameter of the

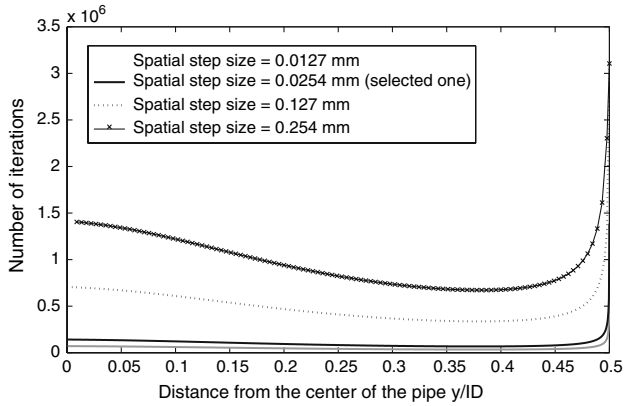

Fig. 9 Number of iterations for different spatial step sizes for the calculation of α_2

acrylic pipe, and the pipe wall thickness. As mentioned previously, an acrylic pipe with an inner radius of 28.575 mm and wall thickness of 12.7 mm was used in this study, therefore $x_f = 41.275$ mm. The coordinates of the contour shape, (x_2,y_2), were solved numerically by iterating a solution that converged when OPL = 56.93 mm. This was performed by guessing a series of values for (x_2,y_2), and the correct values were those that yielded OPL(y_2) = 56.93 mm. The angle α_3 does not appear explicitly in Eqs. 22–29, but is referred to implicity in Eqs. 19–21 in Sect. 3.1.2.

The numerical solution was performed by establishing a value of zero for α_2, as described in Sect. 3.1.2, and OPL = 56.93 mm, with a spatial step size of $\Delta s =$ 0.0254 mm in the numerical approximation to Eq. 22. Figure 9 shows the number of iterations for different values of spatial step size, Δs. The maximum number of iterations (3×10^6 took approximately 5 s when evaluated using a 701 MHz AMD Athlon 64 processor). Figure 9 indicates that the number of iterations is dependent on step size, and that a step size of 0.0254 mm or less results in an accepTable number of iterations given the computational resources that were available at the time of the investigation.

Thus, the shape of the optical contour was calculated, and is shown in Fig. 10. The coordinates of the outer wall, (x_2,y_2) accurately describe the profile of the optical contour that corrects for refraction for imaging of an interior set of collimated beams on a perpendicular plane outside the pipe.

3.2 Ray-tracing tool

Numerical tests were performed on this OCC-computed contour shape by developing a ray-tracing tool (ray-tracker). The ray-tracing tool is a program written to perform a ray trace analysis through an optical system

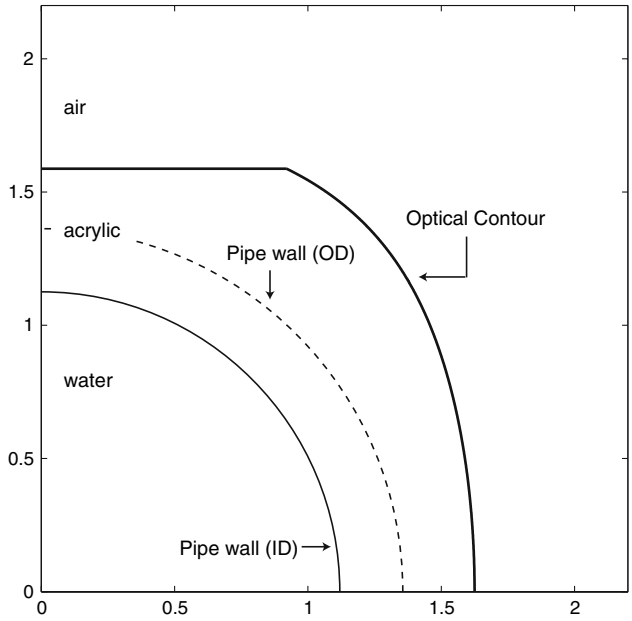

Fig. 10 Optical contour shape

calculated by the OCC. This program is based on ray-tracing techniques (Klein 1970). The program observes how light refracts as it comes into contact with different materials.

3.2.1 *Index of refraction*

A He–Ne laser with wavelength $\lambda = 632.8$ nm is used to generate the optical signal. The values for the index of refraction at this wavelength for standard atmospheric conditions (1 atm and 25°C) were obtained (Weber 2002) for air ($n_{\text{air}} = 1.00027$), water ($n_{\text{water}} = 1.33$) and acrylic ($n_{\text{acrylic}} = 1.49$).

3.2.2 *Ray-tracing equations*

Ray-tracing techniques are used to determine the path that a ray of light takes as it travels through media with index-of-refraction variations. The ray-trace equation (Klein 1970) is given by:

$$\vec{\tau_2} = \frac{n(\vec{r_1})}{n(\vec{r_2})}\vec{\tau_1} + \frac{\Delta s}{n(\vec{r_2})}\nabla n \tag{30}$$

where the gradient operator is defined as:

$$\nabla n = \frac{\partial n}{\partial x}\hat{i} + \frac{\partial n}{\partial y}\hat{j} + \frac{\partial n}{\partial z}\hat{k} \tag{31}$$

The terms used in Eqs. 30 and 31 are graphically illustrated in Fig. 11. A nonzero gradient of the refractive index

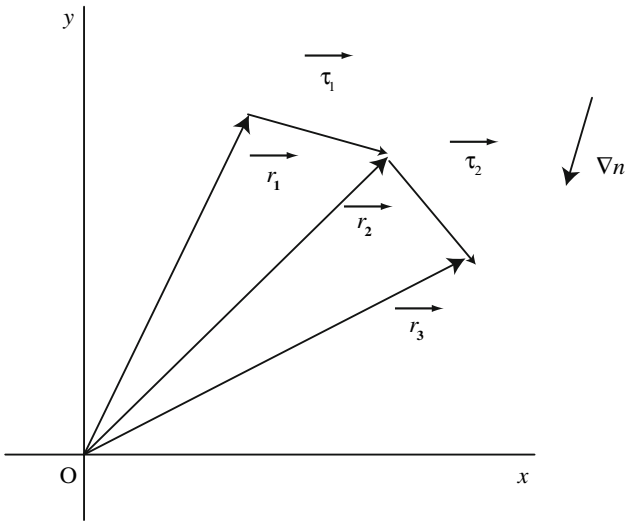

Fig. 11 Symbol conventions for the ray-tracing equations

causes the ray direction $\overrightarrow{\tau_2}$ to be nonparallel to $\overrightarrow{\tau_1}$. Knowing the ray direction at $\overrightarrow{r_2}$ allows one to approximate $\overrightarrow{r_3} = \overrightarrow{r_2} + \overrightarrow{\tau_2}\triangle s$, and so on.

3.2.3 Ray-tracing algorithm

Having formulated an optical system on paper, one can mathematically project beams of light through the system to evaluate its performance. Testing was done for different optical systems including prisms, rectangles, circles, pipe geometry, and finally for a pipe fitted with the optical contour (calculated from the OCC). The ray-tracing tool successfully predicts the path that a beam of light will take when traveling through an optical assembly. The effectiveness of the optical contour shape computed in Sect. 3.1.3 was verified using the ray-tracing program. Figure 12a illustrates the test case where a planar optical wavefront originates from the center of the acrylic pipe and propagates through half of the optical system. Figure 12b illustrates the test case where a planar optical wavefront propagates through the entire optical system. In both test cases, the rays of light travel parallel to each other upon exiting the optical system. The slight deviations of the emerging light rays shown in Fig. 12b are due to numerical approximations from the ray-tracing program. Thus, it was verified that the optical wavefront emerged planar from the optical contour section.

3.2.4 Fresnel equations

The Fresnel equations, derived by Augustin-Jean Fresnel (Welford 1991), describe the amount of light reflected and transmitted at an interface between media of differing refractive indices. When light transmits from a medium of a given refractive index n_1 into a second medium with refractive index n_2, both reflection and refraction of the light may occur, as shown in Fig. 13. For s-polarized light (the electric field vector perpendicular to the plane of incidence), the expression for the complex amplitude reflectance is given by:

$$r_s = \frac{n_1\cos(\theta_i) - n_2\cos(\theta_t)}{n_1\cos(\theta_i) + n_2\cos(\theta_t)} \tag{32}$$

where θ_t can be derived from θ_i by Snell's law. In addition to these field amplitude ratios, one can define the reflected power coefficients (intensity reflectance for s-polarized light) as follows:

$$R_s = |r_s|^2 \tag{33}$$

If the incident light is polarized in the plane of incidence, p-polarized, the expressions are given by:

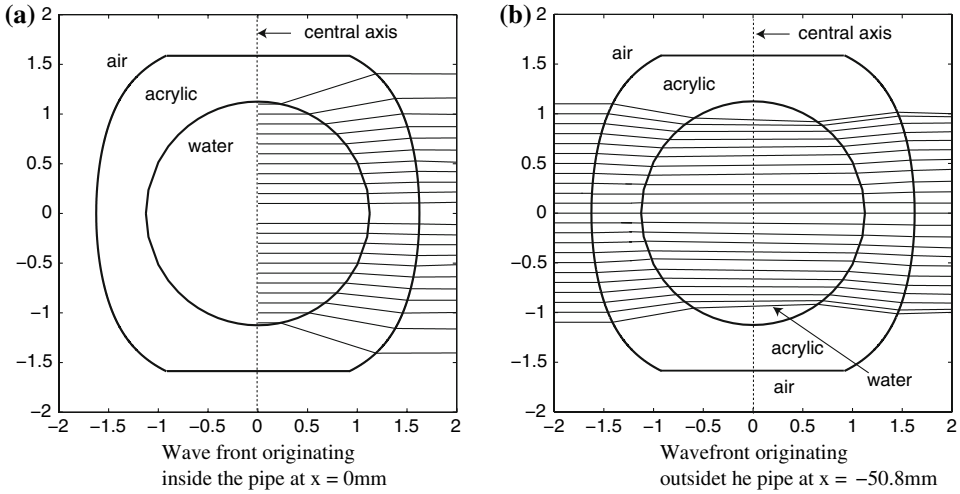

Fig. 12 Ray-trace through an optical contour

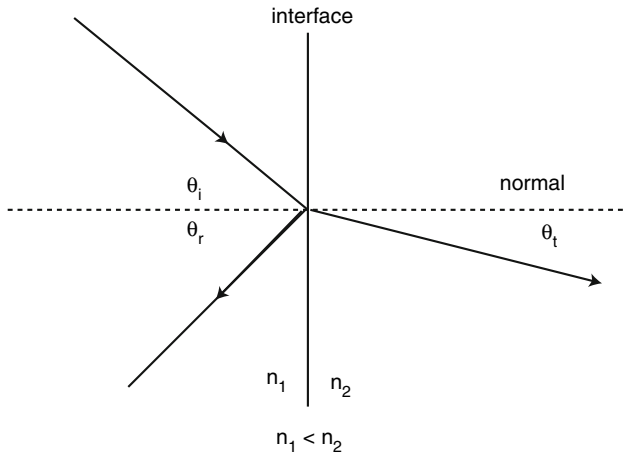

Fig. 13 Light traveling through different media

$$r_{\mathrm{p}} = \frac{n_2 \cos(\theta_i) - n_1 \cos(\theta_t)}{n_1 \cos(\theta_t) + n_2 \cos(\theta_i)} \tag{34}$$

$$R_{\mathrm{p}} = \left|r_{\mathrm{p}}\right|^2 \tag{35}$$

The transmitted power coefficients in each case are given by $T_{\mathrm{s}} = 1 - R_{\mathrm{s}}$ and $T_{\mathrm{p}} = 1 - R_{\mathrm{p}}$. Power transmission coefficients were calculated for four different scenarios:

1. Rays of light propagating through an air–acrylic interface
2. Rays of light propagating through an acrylic–air interface
3. Rays of light propagating through a water–acrylic interface
4. Rays of light propagating through an acrylic–water interface.

Since we are considering behavior in the first quadrant, transmission coefficients as a function of *y*-axis position in the pipe are plotted for water–acrylic, acrylic–air using the pipe only and acrylic–air using the optical contour, illustrated in Figs. 14, 15, 16. Note, at one particular angle for a given n_1 and n_2, the value of T_{p} goes to 100% and a p-polarized incident ray is purely refracted. This is known as the Brewster angle, represented as θ_{B}. When moving from a more to a less dense medium (i.e. $n_1 > n_2$), above an incidence angle known as the critical angle, all light is reflected and $T_{\mathrm{s}} = T_{\mathrm{p}} = 0$. This phenomenon is known as total internal reflection.

From these calculations it is shown that transmission is not an issue unless measurements need to be taken close to the pipe wall. Figure 17 shows the area where optical viewing begins to degrade. Dotted lines indicate the range where the transmission coefficients, T_{s} and T_{p}, remain above 85%. As can be seen, it is challenging for side-view non-invasive fluid-flow imaging experiments to collect data near the walls of the pipe due to the poor transmission characteristics in these regions.

4 Manufacturing

The optical contour is machined as an independent piece that can be placed onto the pipe. The functional specifications of the optical contour must provide high transmissitivy/clarity ratings and show little hazing. Table 1 shows the optical properties of some transparent materials. Standard acrylic was deemed the most appropriate choice of material for the optical contour considering

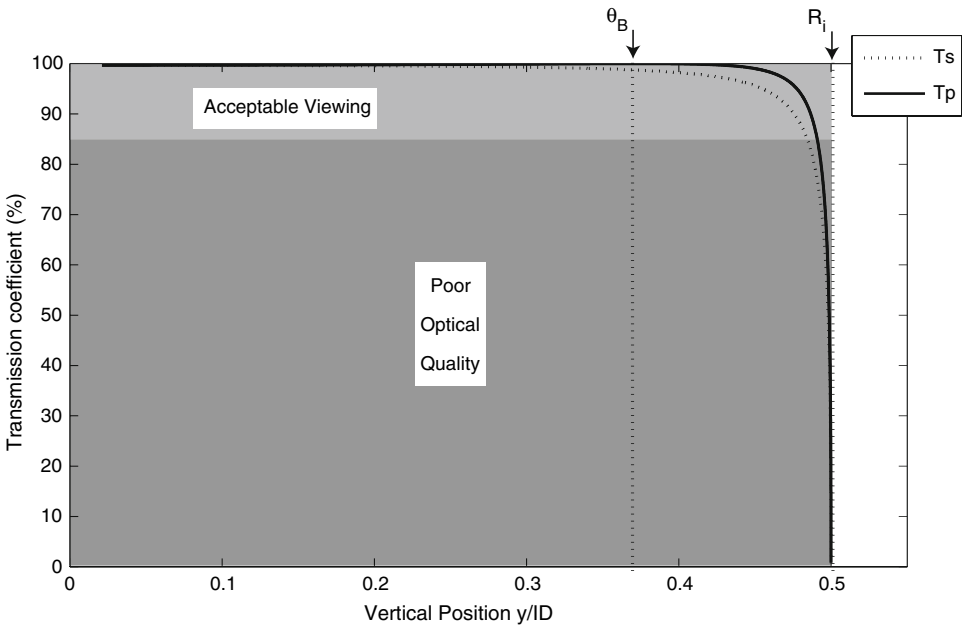

Fig. 14 Transmission coefficients through a water–acrylic interface

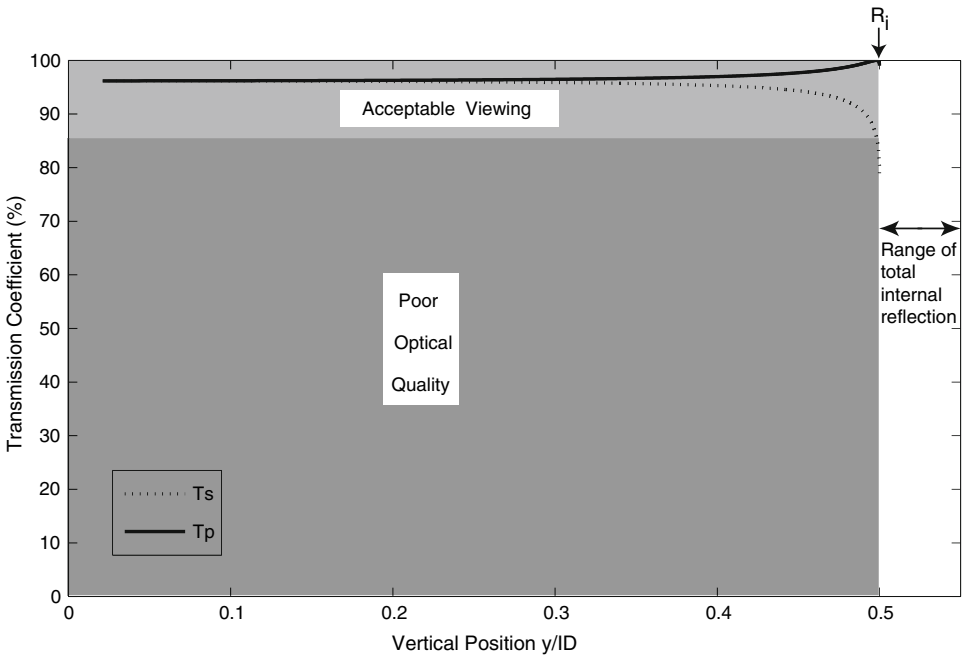

Fig. 15 Transmission coefficients through an acrylic–air interface considering only the pipe as the interface

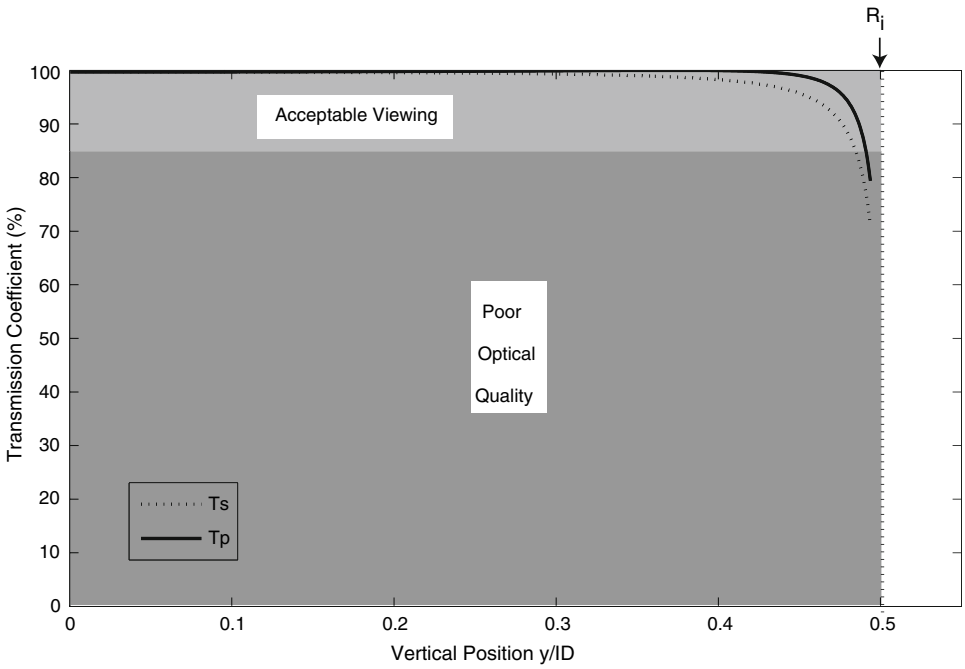

Fig. 16 Transmission coefficients through an acrylic–air interface considering the optical contour as the interface

its optical properties, strength, and performance properties such as chemical and heat resistance, and ease of fabrication.

Coordinates of the optical contour shape, generated from the OCC, were imported into Mastercam G-code for simulation and machining on a 5-axis computer numerically controlled (CNC) machine. G-code is a common name for the programming language that drives CNC machine tools. Manufacturing took place under a 0.79 mm $\left(\frac{1}{32}\text{in.}\right)$ ball nose end mill, with A-9 lubrication oil. The manufactured face then was polished by hand to remove surface imperfections and opaqueness. Using diamond paste solution, the polishing stages were reduced incrementally from 15 to 1 μm. This significantly improved the quality of the finish, while minimizing alterations made to the contoured surface.

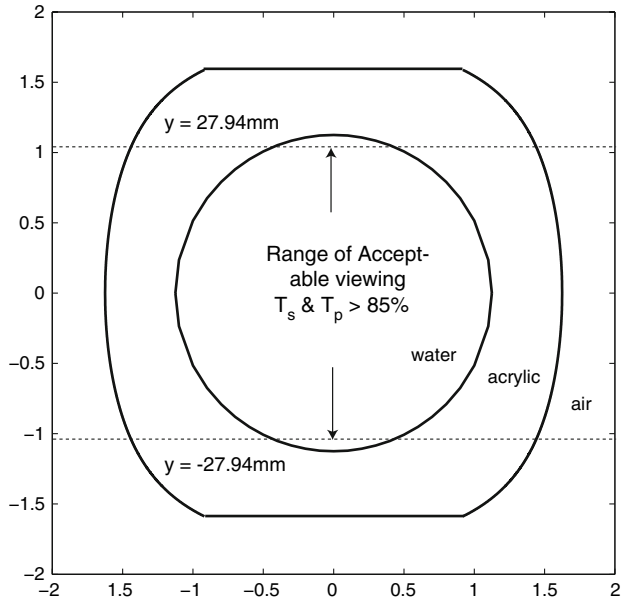

Fig. 17 Range of optical viewing

Table 1 Optical properties of various materials (Weast 1971)

Material	Transmittance (%)	Haze (%)	Refractive index
Glass	92	0–0.17	1.52
Polycarbonate	86–89	1–3	1.586
Standard scrylic	92	2	1.49
TYRIL SAN	87	3	1.57

5 Evaluation of optical contour design

The effectiveness of the optical contour was determined by analyzing the distortion of the emerging optical wavefront. As discussed previously, after transmitting through an optically active medium a light ray will emerge with an off-axis angle θ. This off-axis angle will be equal to the local slope of the emerging wavefront. Experimental quantification of this angle was performed using a small-diameter laser beam and a lateral-effect detector to measure the beam's off-axis angle upon emerging from an acrylic half-pipe, shown in Figs. 18 and 19. The objective was to determine the accuracy of the software in predicting the shape of the optical contour and to quantify the wavefront distortion for three test cases:

1. Acrylic half-pipe with no enclosed liquid, no optical contour
2. Acrylic half-pipe filled with water, no optical contour
3. Acrylic half-pipe/optical contour assembly filled with water.

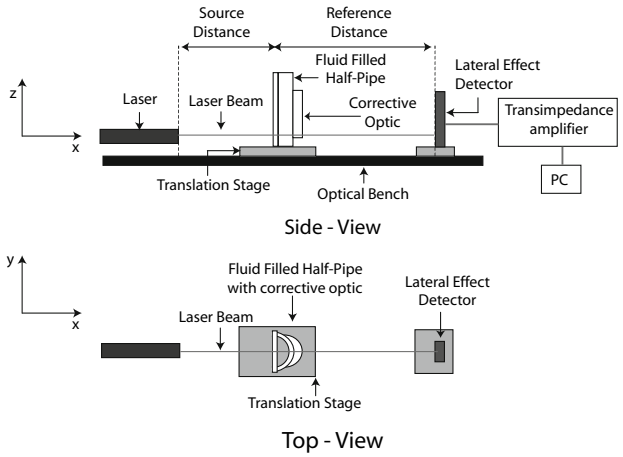

Fig. 18 Experimental apparatus for verification of optical contour design

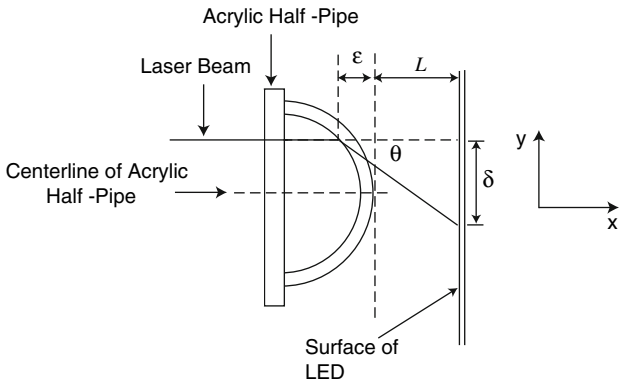

Fig. 19 Wavefront distortion calculation for an acrylic half-pipe where θ is an angle that takes into account the complete deviation of the beam from the inside of the pipe to the LED (deviation due to the pipe plus the deviation due to the air)

5.1 Testing apparatus

A schematic of the optical bench layout is given in Fig. 18. Measurements of the off-axis angle were made with optical components mounted onto an optical bench. The acrylic half-pipe (63.5 mm OD, 57.15 mm ID) was placed on a translation stage that was capable of controlling one-dimensional movements of the half-pipe into and out of the plane of the page, as shown in Fig. 18.

5.1.1 Lateral effect detector

The lateral effect detector (LED) used in the experiment was a Graseby Optronics Model 1233 (SC-10D) that has a 10 mm × 10 mm active sensing area. A LED is a large-

area photodiode that can measure the centroidal location of an incident laser beam. Since the LED is a photodiode, it will induce a current when photons come into contact with its surface. The resulting current will be proportional to the intensity of the incident light, and will also indicate the centroidal location of the incident laser beam. A transimpedance amplifier converts the current into a voltage. The position of the laser beam can then be quantified and recorded.

The method of calibration for the LED consisted of placing the lateral-effect detector onto a y–z translational stage (0.0254 mm resolution) and traversing the detector in both the vertical and horizontal direction with the beam position fixed spatially. When performing a y-axis translation, the voltage corresponding to the z-axis position was kept fixed, and vice versa. The calibration was seen to become non-linear near the largest displacements, and thus the data was fit to a cubic function.

5.1.2 Light source

The light source used was a 1 mW Helium–Neon laser with λ = 632.8 nm. It was not possible to experimentally reproduce bona fide light rays, however the diameter of the laser beam used in this experiment ($\approx$1 mm) is a close estimate, and was used to characterize light rays. In connection with the experimental procedure, the exact center position of the half-pipe was located by translating the half-pipe so that the laser beam transmitted through the central region of the half-pipe. Due to reflection of the laser beam off of the LED, it was possible to align the position of the half-pipe such that the retro-reflection exactly coincided with the incident beam. This ensured that the laser beam was passing precisely through the center of the pipe. Once the pipe was centered, the position of the emerging laser beam was recorded on a PC using a LabVIEW-based data acquisition system. From this reference, the pipe was translated at 0.127 mm increments while recording the position of the emerging laser beam on the LED. Since the LED was placed a known distance L away from the outer edge of the pipe, the off-axis angle of the beam was calculated knowing the off-axis displacement, δ, of the beam:

$$\theta(y) = \tan\left(\frac{\delta}{L+\varepsilon}\right) \tag{36}$$

The geometry of the problem is defined in Fig. 19. The deviation of the beam due to the pipe wall was neglected; ε was calculated from the inside of the pipe to the centerline of the pipe. The beam was considered to follow a straight trajectory from the inside of the pipe and θ was calculated from the point where the beam intersects the inside of the pipe. As mentioned earlier, θ was calculated for three test cases: (1) an acrylic half-pipe with no enclosed liquid; (2) an acrylic half-pipe filled with water; and, (3) an acrylic half-pipe/optical contour assembly filled with water.

5.2 Wavefront distortion

From Huygens' principle it is known that the off-axis angle of the beam, shown in Fig. 19, is equal to the local spatial derivative of the optical wavefront. It can be shown that for $\theta(y) \ll 1$, the OPL is given as (Jumper and Fitzgerald 2001):

$$\frac{\mathrm{dOPL(y)}}{\mathrm{dy}} = -\theta(y) \tag{37}$$

The negative sign appears in front of $\theta(y)$ because the OPD and optical wavefront are conjugates. Integrating this equation with respect to y yields:

$$\mathrm{OPL}(y) = -\int_{y_1}^{y_2} \theta(y)\mathrm{dy} \tag{38}$$

This is an equation for the OPL at the location of the laser beam. The integral may be approximated numerically with great accuracy, seeing that $\theta(y)$ was interrogated every 0.127 mm ($u_\delta = \pm 0.0002$ mm, $u_\theta = \pm 2.459 \times 10^{-6}$). Using Eq. 2, the OPD can be calculated from the OPL, and hence, the emerging optical wavefront can be estimated with uncertainty $u_{\mathrm{OPD}} = \pm 0.01753$ μm. Figure 20 shows the shape of the emerging optical wavefronts across the entire ID of the half-pipe for test case (2) and (3), mentioned previously in Sect. 5.

The trend for an acrylic half-pipe filled with water, shown as a dotted line in Fig. 20, suggests the wavefront is converging upon exiting the pipe. The trend for an acrylic half-pipe/optical contour assembly filled with water, shown

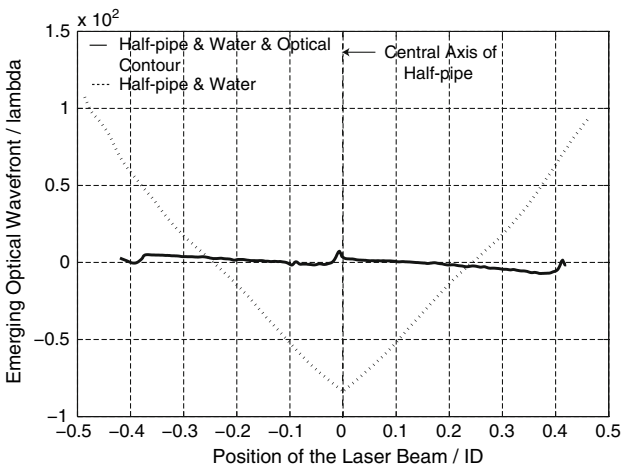

Fig. 20 Emerging wavefront distortion

as a solid line, shows the wavefront is relatively planar when emerging from the optical system. This is in good agreement with the ray-trace results shown in Sect. 3.2.3. This demonstrates that the contoured acrylic surface is altering the character of the emerging optical wavefront such that it is planar.

The peak-to-peak value of the optical wavefront in the data set shown for an acrylic half-pipe filled with water was 1.31×10^5 nm. When this value is compared to the wavelength of the He–Ne laser beam used in the experiment, 632.8 nm, the optical wavefront is shown to be equivalent to $207\lambda_{\text{He–Ne}}$. However, the peak-to-peak value of the optical wavefront in the data set shown for an acrylic half-pipe/optical contour assembly is 6.52×10^3 nm. When compared to the wavelength of the He–Ne laser beam, the optical wavefront is shown to be corrected to $10\lambda_{\text{He–Ne}}$, a significant improvement.

5.3 Grid test

The effect of wavefront distortion was studied further by fixing a uniform square grid (2.5 mm × 2.5 mm) on the flat wall within the acrylic half-pipe described in Sect. 5.1. By filling the acrylic half-pipe with water to a certain level, and covering only a certain portion of the pipe wall with the optical contour, an image of the grid distortion when imaged through various media may be examined. When attaching the optical contour to the pipe wall, proper alignment is important and can be achieved by using common optical alignment techniques (alignment of retroreflective beam with incident beam, for instance). Figure 21 shows an image of the grid distortion for four interface scenarios: (1) air; (2) air and the acrylic half-pipe; (3) water and the acrylic half-pipe; and, (4) water, the acrylic-half pipe, and the optical contour. From the image shown in Fig. 20, interface scenario (3) is clearly more aberrated than interface scenario (4), and this is credited to the optical contour providing correction.

The photograph shown in Fig. 21 was imported into Adobe Photoshop 7.0. The number of pixels defining height and width of each grid were counted for each of the four interface scenarios. The number of pixels defining grid height and width for interface scenario (1) was found to be undistorted. However, the number of pixels defining the width of each grid for the other three interface scenarios were found to vary across the entire viewing aperture of the half-pipe (the number of pixels defining height of each grid were found to be constant). The grid distortion for interface scenario (3) and (4) were compared by examining the variation of the number of pixels in each grid, as shown below in Eq. 39:

$$\%\text{Error} = \frac{\text{Pixels}_{\text{distorted}} - \text{Pixels}_{\text{undistorted}}}{\text{Pixels}_{\text{undistorted}}} \times 100 \qquad (39)$$

where $\text{Pixels}_{\text{distorted}}$ are the number of pixels counted for each grid, and $\text{Pixels}_{\text{undistorted}}$ are the number of pixels in a grid in the undistorted interface scenario (1). This quantification of grid distortion is plotted as a function of the centroidal location of each grid with respect to the central axis of the half-pipe, illustrated in Fig. 22. Interface scenario (3) is shown to be altered approximately 40% across the entire viewing aperture of the half-pipe. However, the optical contoured section is distorted less than 10% in the

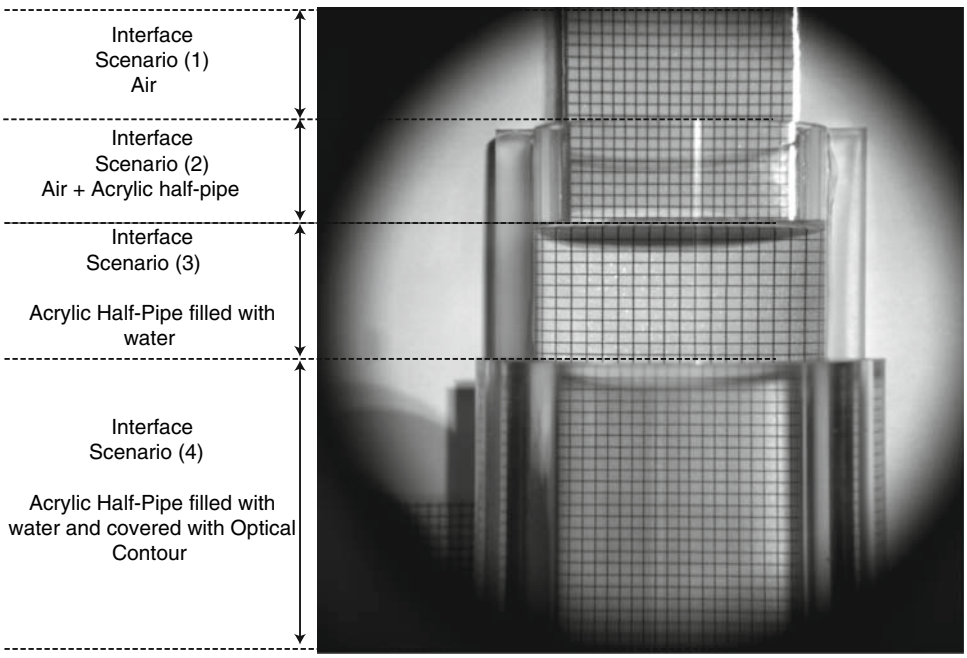

Fig. 21 Image distortion of a uniform square grid through an acrylic half-pipe

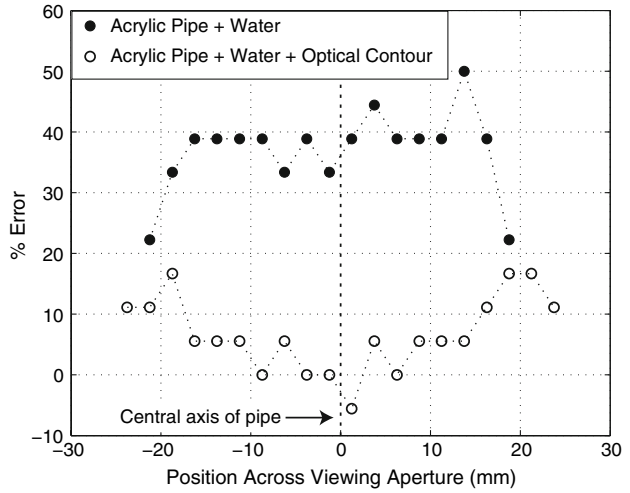

Fig. 22 Quantification of the image distortion of (1) an acrylic half-pipe filled with water and (2) an acrylic half-pipe filled with water and covered with the optical contour. The distortion of each grid is plotted as a function of the centroidal position of each grid with respect to the center of the viewing aperture

central region and close to 20% near the pipe edges, a considerable improvement.

6 Conclusions

The focus of this work was to custom machine an acrylic surface that corrects for optical aberrations. Experiments were performed to measure the emerging optical wavefront for three test cases. The data collected shows that for an optical assembly consisting of an acrylic half-pipe filled with water and an optical contour, that the emerging optical wavefront is planar. When compared to the emerging wavefront of a pipe filled with water, major improvements were shown. The peak-to-peak value of the optical wavefront through an acrylic half-pipe filled with water was $207\lambda_{\mathrm{He-Ne}}$, whereas for an acrylic half-pipe/optical contour assembly, the peak-to-peak value of the emerging optical wavefront was $10\lambda_{\mathrm{He-Ne}}$. This demonstrates that optical contouring promises to be an effective method in reducing optical distortions due to a curved surface. This paper has successfully shown the design methodology behind the computation, manufacturing, and testing of an optically contoured acrylic surface for use in pipe-flow investigations.

There are two areas for future direction in this work. The first direction involves experimenting with more efficient and less expensive means of manufacturing the optical contour. This would involve custom machining a mold of the optical contour, and using liquid acrylic in conjunction with a "hardening" agent to produce optically contoured surfaces. A second and more immediate direction involves the final evaluation of the optical contouring method for application in other pipe-flow imaging experiments that include optical tomography, particle image velocimetry, and imaging with high speed digital-video cameras.

Acknowledgments This research has been made possible by funding through the support of a National Sciences and Engineering Research Council of Canada (NSERC) Discovery Grant. Thanks to A. Vicharelli of Stanford University for her timely advice on design methodology, manufacturing & polishing. Also, thanks to Dr. Kahn of the University of Calgary for generously donating diamond paste that ultimately led to the timely completion of this study.

References

Agrawal Y, Talbot L, Gong K (1978) Laser anemometer study of flow development in curved circular pipes. J Fluid Mech 85(3):497–518

Bertola V (ed) (2004) Modelling and experimentation in two-phase flow. Springer, Heidelberg

Bicen A (1982) Refraction corrections for lda measurements in flows with curved optical boundaries. TSI Q

Boadway J, Karahan E (1981) Correction of laser doppler anemometer readings for refraction at cylindrical interfaces. DISA Inf 26:4–6

Chan V, Delaure Y, Murray D, Fitzpatrick J (2004) Optical considerations for time-resolved digital piv measurement in single bubble flow against heated boundaries. Meas Sci Tech 15:N39–N42

Durrett R, Gould R, Stevenson W, Thompson H (1985) A correction lens for laser doppler velocimeter measurements in a cylindrical tube. AIAA J 23(9):1387–1391

Dybbs A, Edwards R (1987) Refractive index matching for difficult situations. In: 2nd International confreence on laser anemometry, advances and applications

Els H, Rouve G (1985) Ldv measurements in pipe-flow problems and experimences. In: ASME 2nd international symposium on laser anemometry, Miami Beach, pp 293–298

Giancola D (1984) General physics. Prentice Hall Inc., Englewood Cliffs

Jumper E, Fitzgerald E (2001) Recent advances in aero-optics. Progr Aero Sci 37:299–339

Klein MV (1970) Optics. Wiley, New York

Laskowski G, Vicharelli A, Medic G, Elkins C, Eaton J, Durbin P (2005) Inverse design of and experimental measurements in a double-passage transonic turbine cascade model. J Turbomach 127(3):619–626

Lowe M, Kutt P (1992) Refraction through cylindrical tubes. Exp Fluids 13:315–320

Lowe M, Kutt P, York T, Kazonov L, Leavy B (1993) Reconstruction of three-dimensional particle trajectories in flows through curved circular tubes. Exp Fluids 14:402–408

Maanen H, Fortuin J (1983) Experimental determination of the random lump-age distribution in the boundary layer of the turbulent pipe flow using laser doppler anemometry. Chem Eng Sci 38:399–423

McMackin L, Masson B, Clark N, Bishop K, Pierson R, Chen E (1995) Hartmann wave front sensor studies of dynamic organized structure in flowfields. AIAA J 33(11):2158–2164

McMackin L, Hugo R, Bishop K, Chen E, Pierson R, Truman C (1999) High speed optical tomography system for quantitative measurement and visualization of dynamic features in a round jet. Exp Fluids 26:249–256

Mizushina T, Usui H (1977) Reduction of eddy diffusion for momentum and heat in viscoelastic fluid flow in a circular tube. Phys Fluid 20:S100–S108

Pereira J, Sousa J (1999) Confined vortex breakdown generated by a rotating cone. J Fluid Mech 385:287–323

Steenbergen W (1996) Reduction of beam refraction in optical pipe flow experiments by use of sheet fabricated pipe walls. Exp Fluids 22:165–173

Uzol O, Chow Y, Katz J, Meneveau C (2002) Unobstructed particle image velocimetry measurements within an axial turbo-pump using liquid and blades with matched refractive indices. Exp Fluids 33:909–919

Weast R (1971) CRC Handbook of Chemistry and Physics, 52nd edn. The Chemical Rubber Company

Weber M (2002) Handbook of optical materials. CRC Press, Boca Raton

Welford W (1991) Useful optics. The Chicago Lectures in Physics. University of Chicago Press, Chicago

Wendt C, Mickan B, Kramer R, Dopheide D (1996) Systematic investigation of pipe flows and installation effects using laser doppler anemometry- part i. profile measurements downstream of several pipe configurations and flow conditioners. Flow Meas Instrum 7(3/4):141–149

Westerweel J, Draad AA, van der Hoeven J, van Oord J (1996) Measurement of fully-developed turublent pipe flow with digital particle image velocimetry. Exp Fluids 20:165–177

Zhang Z (2004) Particle image velocimetry (piv) measurements of an inline pipe vortex. Master's thesis, University of Calgary